Journal of Manufacturing Innovations
2025, VOL. 1, NO. 3, 30–39
DOI: 10.22055/jomi.2025.49568.1029

Electrochemical Corrosion Performance of FeCoNiCr Medium-Entropy Alloy in Neutral, Acidic, and Saline Solutions

N. Hedayati, Y. Heidari, Kh. Gheisari*, M. Yeganeh
Department of Materials Science and Engineering, Faculty of Engineering, Shahid Chamran University of Ahvaz, Ahvaz, Iran

ABSTRACT

This study investigates the microstructure and corrosion behavior of a vacuum arc melted FeCoNiCr medium-entropy alloy in various aqueous environments, including deionized water, 1 M sulfuric acid, and 4 wt.% sodium chloride solutions. Microstructural analysis revealed a hierarchical architecture composed of large equiaxed grains (approximately 100–400 μm) featuring a cellular substructure. Potentiodynamic polarization tests demonstrated that the alloy exhibited significantly lower corrosion resistance in the sulfuric acid environment, with a corrosion current density of 39.81 $\mu A \cdot cm^{-2}$, compared to much lower values in deionized water (0.07 $\mu A \cdot cm^{-2}$) and sodium chloride solution (0.08 $\mu A \cdot cm^{-2}$). Notably, in the NaCl solution, the alloy displayed strong passivation behavior, characterized by a broad passivation range of 1146 mV and a low passive current density, closely matching its performance in deionized water. These results highlight the alloy's excellent corrosion resistance in chloride-containing environments.

ARTICLE HISTORY
Received 5 May 2025
Revised 22 June 2025
Accepted 12 July 2025

KEYWORDS
Medium-entropy alloy
FeCoNiCr
Potentiodynamic polarization
Passivity
Sulfuric acid
Sodium chloride.

1. Introduction

High-entropy alloys (HEAs), also known as multi-principal element alloys (MPEAs), are a class of materials typically composed of five or more principal elements in equimolar or near-equimolar ratios, first introduced by Yeh et al. and Cantor et al. in 2004. Derived from the same design philosophy, medium-entropy alloys (MEAs) contain fewer principal elements—usually three or four—yet still exhibit the unique structural and functional characteristics associated with high configurational entropy, making them attractive candidates for advanced engineering applications [1, 2]. From a thermodynamic perspective, the high mixing entropy minimizes the Gibbs free energy, thus stabilizing the formation of solid solution phases even when elements with different crystal structures are involved [3].

HEAs and MEAs often exhibit simple microstructures, typically consisting of face-centered cubic (FCC), body-centered cubic (BCC), or hexagonal close-packed (HCP) solid solutions [4, 5]. Unlike conventional alloys where one or two elements dictate the overall structure, the properties of these alloys can be tailored by carefully selecting and controlling the constituent elements. For instance, the selection of elements with significant differences in atomic size can lead to substantial lattice distortion, which contributes to enhanced strength and hardness [6, 7]. Hence, the properties of these alloys are significantly influenced by their composition and resulting microstructure.

Numerous studies have investigated the influence of various alloying elements on the corrosion behavior of high-entropy alloys. The corrosion resistance of HEAs is largely governed by the presence and combination of specific elements, which can significantly affect the formation, stability, and protectiveness of passive oxide films on the alloy surface. Elements such as chromium (Cr), molybdenum (Mo), and titanium (Ti) are particularly effective in enhancing corrosion resistance by promoting the development of stable and adherent passive layers, especially in aggressive environments like acidic or saline solutions. These passive films serve as protective barriers, reducing metal dissolution and improving overall durability [8]. The influence of other elements—including tungsten (W), cobalt (Co),

* Corresponding author.
E-mail address: khgheisari@scu.ac.ir (Kh. Gheisari)

and aluminum (Al)—has also been examined in relation to their role in modifying corrosion performance. Several studies have reported that HEAs can exhibit significantly lower corrosion rates compared to conventional materials such as 304 stainless steel in specific environments [9, 10]. Additionally, targeted investigations have explored the individual effects of alloying elements such as titanium [11], tungsten [12], molybdenum [13], chromium [14], and boron [15] on the corrosion behavior of HEAs, further highlighting the importance of compositional design in optimizing corrosion resistance.

The equimolar FeCoNiCr medium-entropy alloy is considered relatively simple in terms of its elemental composition and can be readily synthesized. It typically forms a stable single-phase solid solution, thereby avoiding the complications associated with intermetallic compound formation. Despite its compositional simplicity, the corrosion behavior of FeCoNiCr in various corrosive environments remains insufficiently explored. In this study, we investigate the corrosion behavior of additively manufactured FeCoNiCr alloy produced via vacuum arc melting. Corrosion performance is evaluated in three representative environments: deionized water, 1 M sulfuric acid solution, and 4 wt% sodium chloride solution.

2. Materials and Methods

2.1. Alloy preparation

To fabricate the FeCoNiCr medium-entropy alloy, purity raw bulk materials of iron, cobalt, nickel, and chromium were weighed in equimolar ratios. Based on the designed composition of the alloy investigated in this study, the estimated melting temperature is about 1600 °C. Given the use of a water-cooled copper mold, along with the dimensions and thermal properties of the castings, the solidification cooling rate was estimated to fall within 13–20 °C/s. Prior to arc melting, the raw elemental materials were mechanically polished using sandpaper and cleaned with alcohol to remove any surface contaminants and oxide layers. To minimize oxidation during melting, the vacuum arc melting chamber was initially evacuated to a pressure of 10^{-3} mbar using a mechanical pump. This was followed by repeated purging with high-purity argon gas to ensure a controlled inert atmosphere, maintaining a final pressure below 1 bar. Additionally, a titanium getter was arc-melted inside the chamber to further scavenge residual oxygen, ensuring an oxygen-free environment throughout the process. The cleaned raw materials were then melted using arc melting, and once a homogeneous liquid alloy was achieved, it was cast into a water-cooled copper mold to form cylindrical ingots with approximate dimensions of 15 mm in diameter and 10 mm in height. To enhance chemical homogeneity and microstructural uniformity, each alloy ingot was remelted at least five times.

2.2. Characterization

The as-cast ingots were mechanically ground using silicon carbide (SiC) abrasive papers ranging from #60 to #2000 grit, followed by final polishing with a colloidal alumina suspension. For microstructural analysis, the polished samples were electrochemically etched using a solution of 1 M H_2SO_4 (2.5 mL) and CH_3OH (47.5 mL). The microstructure was analyzed using optical microscopy (OM) and scanning electron microscopy (SEM) combined with energy-dispersive X-ray spectroscopy (EDS). The phase identification was performed using X-ray diffraction (XRD) with Cu Kα radiation (λ=1.5406A˚) in the 2θ range of 30° to 100° at a scanning rate of 0.02°/s. To evaluate the corrosion resistance, the as-cast samples were immersed in three different corrosive solutions: 1 M sulfuric acid (H_2SO_4), 4 wt% sodium chloride (NaCl), and deionized water. Prior to electrochemical measurements, the samples were immersed in the respective solutions for one hour to establish a stable open-circuit potential. Electrochemical measurements were performed using an AutoLab AUT84091 potentiostat in a standard three-electrode cell configuration. A saturated Ag/AgCl electrode was used as the reference electrode, a platinum mesh served as the counter electrode, and the fabricated sample was used as the working electrode. The as-cast ingot had a tablet-like geometry with a height of 5 mm and a diameter of 13.6 mm. To ensure precise evaluation, all other surfaces were covered with an insulating mounting

material, leaving only a centrally positioned square surface area of 10 × 10 mm² on the top face of the samples exposed for corrosion testing. This exposed area was mechanically ground and polished to a mirror finish prior to each experiment. Potentiodynamic polarization tests were performed by scanning the potential from -300 mV below the OCP to +1300 mV above the OCP at a scan rate of 1 mV/s.

3. Results and Discussion

Figure1 presents the XRD pattern of the as-fabricated FeCoNiCr alloy, revealing a characteristic FCC crystalline structure. The diffraction pattern exhibits four distinct peak indices: (111), (200), (220), and (311), which are characteristic of a single-phase FCC solid solution. The (111) plane demonstrates the most intense diffraction peak, consistent with the crystallographic characteristics of transition metal solid solutions. The peak positions and relative intensities precisely match the expected FCC crystal structure, as illustrated by the schematic unit cell representation. The absence of secondary phase peaks indicates complete solid solubility of the constituent elements (Fe, Co, Ni, Cr) within the FCC lattice, suggesting successful alloying and uniform elemental distribution. The sharp, well-defined peaks further suggest high crystallographic order and minimal structural defects, implying a high-quality material with potential for advanced structural or functional applications.

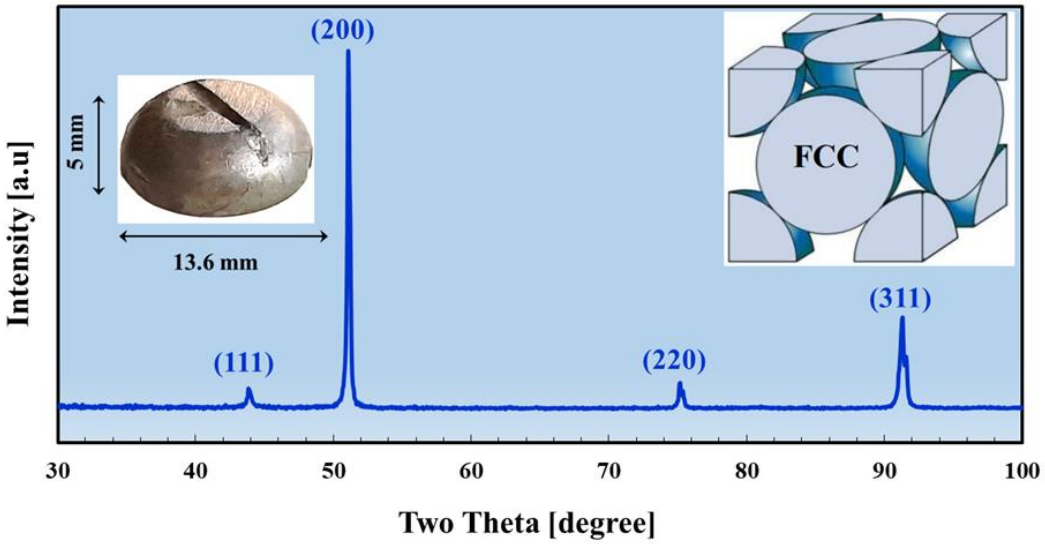


Figure 1. XRD pattern of the FeNiCoCr medium-entropy alloy produced in this study.

Optical microscopy images of the FeCoNiCr medium-entropy alloy at various magnifications, as presented in Figure2, reveal a hierarchical microstructure characterized by large equiaxed grains containing a fine cellular substructure. The coarse grains, with sizes ranging from approximately 100 to 400 µm, suggest the presence of a stable solidification front during cooling—an outcome consistent with the vacuum arc melting process followed by rapid quenching in a water-cooled copper mold. The uniformity in grain size and morphology across the sample indicates effective thermal control and thorough mixing, likely enhanced by repeated remelting cycles during synthesis. Within these grains, a distinct cellular pattern becomes evident at higher magnifications. Although such features are often associated with solute partitioning and microsegregation during non-equilibrium solidification, energy-dispersive X-ray spectroscopy analysis, discussed later in this work, confirms a uniform elemental distribution across different regions of the alloy. The absence of detectable microsegregation suggests that the observed cellular structure arises from solidification dynamics, crystallographic growth directions, or local thermal gradients rather than compositional inhomogeneities. The coexistence of large equiaxed grains and chemically homogeneous cellular substructures underscores the capability of the vacuum arc melting technique to produce medium-entropy alloys with a refined

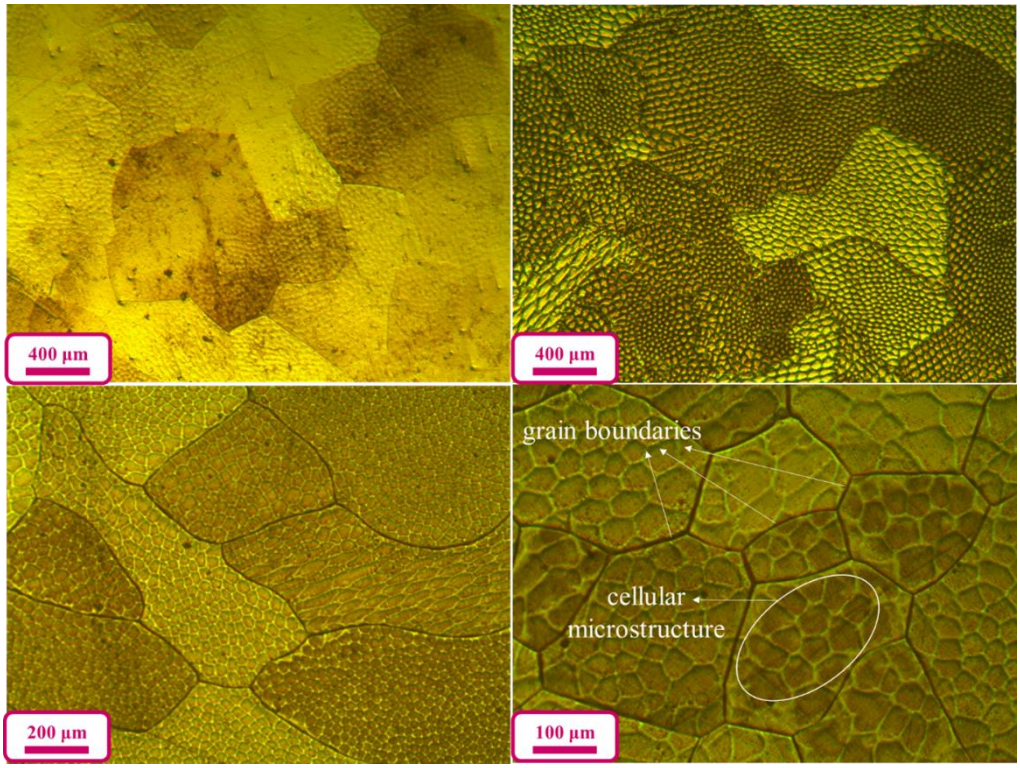


Figure 2. Optical microstructure of the FeNiCoCr medium-entropy alloy at various magnifications.

and uniform microstructure. This structural uniformity is expected to contribute positively to both mechanical performance and corrosion resistance.

The microstructural and compositional analysis of the vacuum arc-melted FeCoNiCr medium-entropy alloy, as shown in Figure 3, confirms the formation of a homogeneous single-phase structure. The SEM image reveals an equiaxed grain structure with well-defined grain boundaries and no visible signs of dendritic segregation or secondary phase formation. EDS measurements at four distinct locations (Points A–D) across the microstructure confirmed a consistent elemental distribution, with atomic percentages ranging from 27.7–28.7% Cr, 27.2–27.9% Co, 22.4–23.5% Fe, and 21.0–21.4% Ni. The minimal compositional variations (±1 at.%) indicate exceptional elemental mixing achieved through the fabrication methodology, which included multiple remelting cycles and water-cooled copper mold casting. The use of a high-purity argon atmosphere, maintained through repeated vacuum purging and the use of a titanium getter to remove residual oxygen, minimized contamination and oxidation during processing. The observed microstructural homogeneity is attributed to the synergistic effects of precise thermal processing and the inherent solid-solution-forming characteristics of the selected transition metals, establishing a stable, single-phase microstructure with potential implications for advanced materials design.

Figure 4 shows the potentiodynamic polarization curves of the produced alloy in three different corrosive environments. The electrochemical corrosion parameters including corrosion potential (E_{corr}), corrosion current density (i_{corr}), passivation current density (i_{pass}: the lowest current density in the passive region of anodic polarization branch [16]), pitting potential (E_{pit}) and passivation potential range ($\Delta E = E_{pit}–E_{pass}$) [17] were determined by analyzing the polarization plots, as summarized in Table 1. The polarization curves and the resultant electrochemical corrosion parameters yield the following observations.

(i) The alloy exhibits distinct electrochemical behavior depending on the corrosive medium. In deionized water and the sodium chloride solution, the alloy demonstrates a tendency for spontaneous

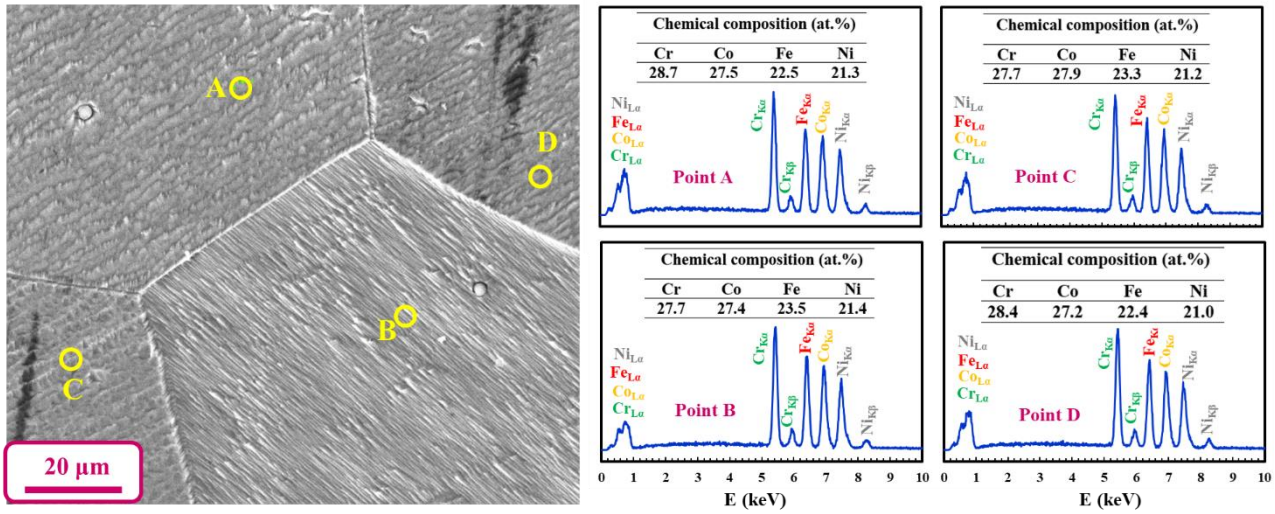


Figure 3. SEM image of the FeCoNiCr medium-entropy alloy, with EDS analysis at multiple points (A–D) confirming a uniform elemental distribution of Cr, Co, Fe, and Ni.

passivation; however, a classic passivation plateau is not observed. Instead, the polarization curves reveal an extended passive region characterized by a relatively low and stable current density over a certain potential range, followed by a sharp increase in current density at higher potentials, indicating the onset of pitting corrosion. This suggests the formation of a protective passive film in both environments, albeit with susceptibility to localized breakdown at elevated potentials. In contrast, the polarization curve in the sulfuric acid solution displays a well-defined passivation behavior. After an initial increase in current density in the anodic branch, the curve reaches a primary passivation potential, beyond which the current density remains nearly constant over a wide potential range. This indicates the formation of a stable and protective passive film, consistent with classical passivation behavior typically observed in acid environments.

(ii) The corrosion potential and corrosion current density were determined by extrapolating the linear segment of the cathodic Tafel region in the polarization curve. The intersection of the extrapolated line provides the corrosion potential, while the current density at this intersection represents the corrosion current. However, obtaining precise measurements can be challenging when the cathodic branches lack clear linear segments, potentially introducing uncertainties in the electrochemical characterization. The obtained values are presented in Figure 5. Generally, the corrosion potential indicates the thermodynamic tendency of a metal to corrode. A more positive corrosion potential suggests a higher thermodynamic stability and a lower tendency for corrosion. However, the corrosion current density is a kinetic parameter that reflects the rate of the corrosion reaction. A lower corrosion current density indicates a higher corrosion resistance.

Based on the polarization curves, the corrosion current density in the 1 M sulfuric acid solution (39.81 $\mu A \cdot cm^{-2}$) is significantly higher than that in deionized water (0.07 $\mu A \cdot cm^{-2}$) and the 4 wt.% sodium chloride solution (0.08 $\mu A \cdot cm^{-2}$). This indicates that the FeCoNiCr medium-entropy alloy exhibits significantly lower corrosion resistance in the sulfuric acid environment compared to the other two environments.

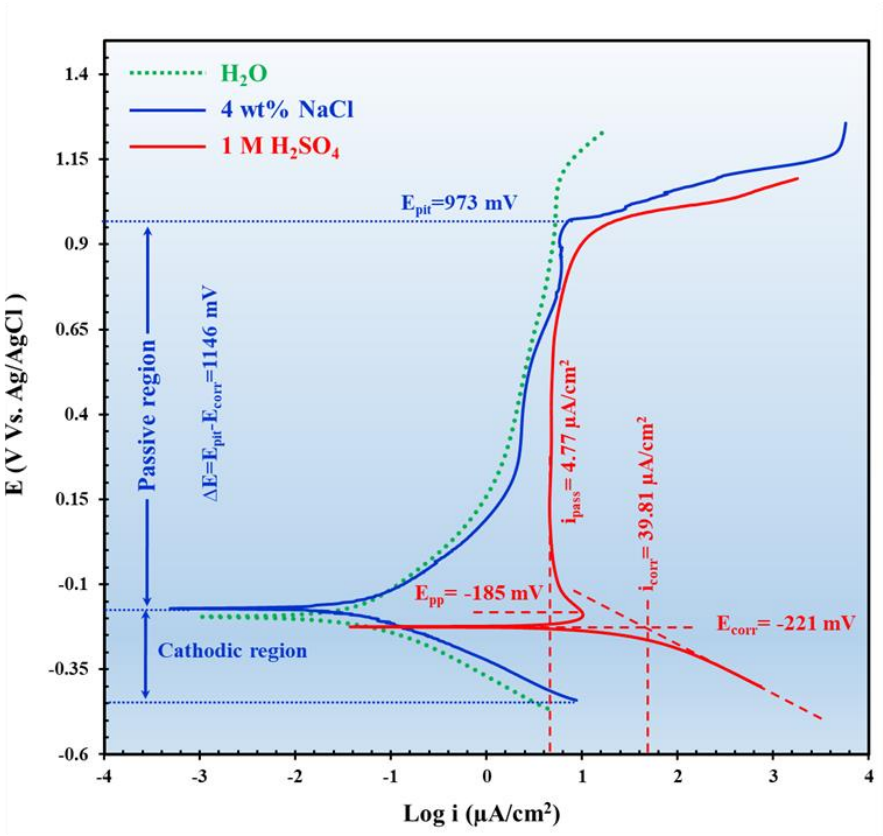


Figure 4. Potentiodynamic polarization curves of the FeCoNiCr medium-entropy alloy in three different solutions: 1 M H_2SO_4, 4 wt.% NaCl, and deionized water.

Table 1. Corrosion parameters obtained from the potentiodynamic polarization curves of the FeNiCoCr alloy in three environments: 1 M sulfuric acid, 4 wt.% sodium chloride solution, and deionized water.

Solution	E_{corr} (mV Vs. Ag/AgCl)	i_{corr} (μA/cm^2)	i_{pass} (μA/cm^2)	E_{pit} (mV Vs. Ag/AgCl)	ΔE (mV)
1 M H_2SO_4	-221	39.81	4.77	956	1177
4 wt.% NaCl	-173	0.76	0.76	973	1146
H_2O	-198	0.07	0.07	1108	1306

(iii) Notably, the corrosion current densities in deionized water and sodium chloride solution are nearly identical and approximately two orders of magnitude lower than that in sulfuric acid, indicating superior corrosion resistance in these media. This result implies that the passive film formed on the surface of the FeCoNiCr alloy is highly effective in neutral and chloride-containing environments, providing considerable protection even in the presence of aggressive chloride ions. The insensitivity of the passive film to chloride ions may be attributed to the alloy's high chromium content, which is known to facilitate the formation of a stable and adherent Cr_2O_3-based passive film. This film likely acts as a protective barrier, preventing aggressive chloride ions from penetrating and initiating localized corrosion. Additionally, the synergistic effect of the equiatomic distribution of transition metals such as Fe, Co, and Ni may enhance the film's

compactness and stability, further improving its resistance to chloride-induced degradation.

(iv) The corrosion potential in the sulfuric acid solution (−221 mV vs. Ag/AgCl) is slightly more negative than that in deionized water (−198 mV vs. Ag/AgCl) and in the sodium chloride solution (−173 mV vs. Ag/AgCl). While a more noble (less negative) corrosion potential generally indicates a greater thermodynamic tendency for passivation and improved corrosion resistance, it is not the sole determinant of corrosion performance. In this case, although the corrosion potential in sulfuric acid is slightly more negative, the significantly higher corrosion current density indicates that the passive film formed in this environment is less stable or more prone to breakdown. Conversely, the more positive corrosion potentials in deionized water and NaCl solution, combined with much lower corrosion current densities, suggest the formation of a more protective and stable passive layer in these environments. Given its relatively good performance in the chloride-containing environment, the FeNiCoCr alloy shows promise as a potential alternative to some conventional stainless steels in specific applications.

(v) To further evaluate the passivation behavior of the FeCoNiCr alloy, key parameters reflecting passive film stability and protectiveness were extracted from the potentiodynamic polarization curves. These include the pitting potential (E_{pit}), the passivation range (ΔE_{pass}), and the passive current density (i_{pass}). A higher pitting potential and a broader passivation range, combined with a lower i_{pass}, are indicative of a more stable and protective passive film. In general, lower passive current densities suggest reduced metal dissolution during passivation, while a wider passivation range and elevated pitting potential reflect the film's resilience to localized breakdown. Together, these parameters provide a comprehensive assessment of the passive film quality and its effectiveness in resisting corrosion under different environmental conditions.

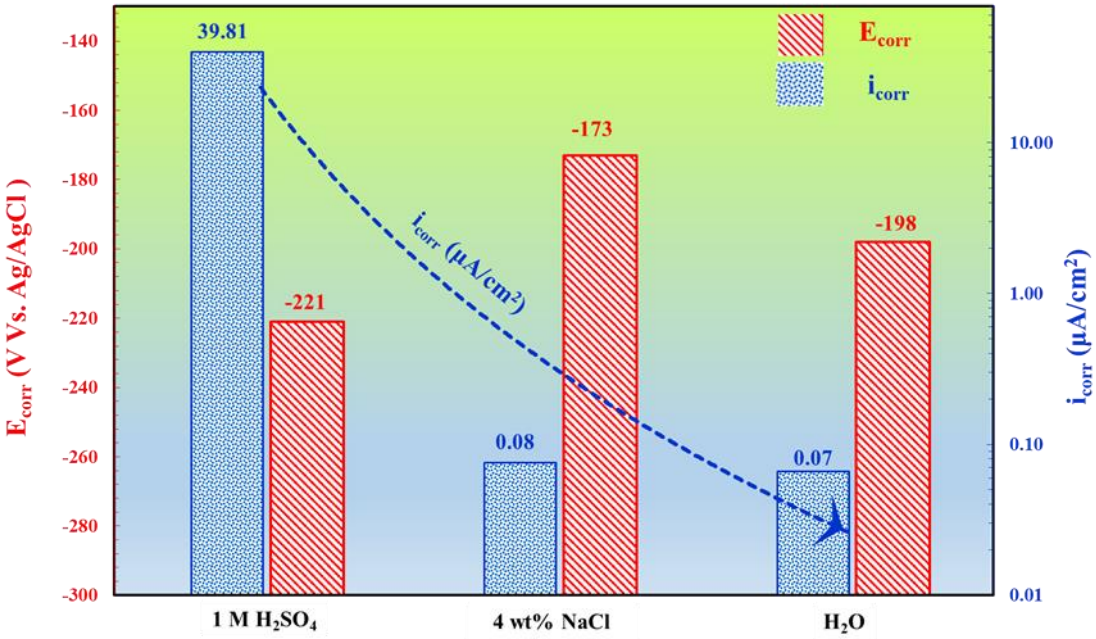


Figure 5. Corrosion potential and corrosion current density extracted from the potentiodynamic polarization curves of the FeNiCoCr alloy in three environments: 1 M sulfuric acid, 4 wt.% sodium chloride solution, and deionized water.

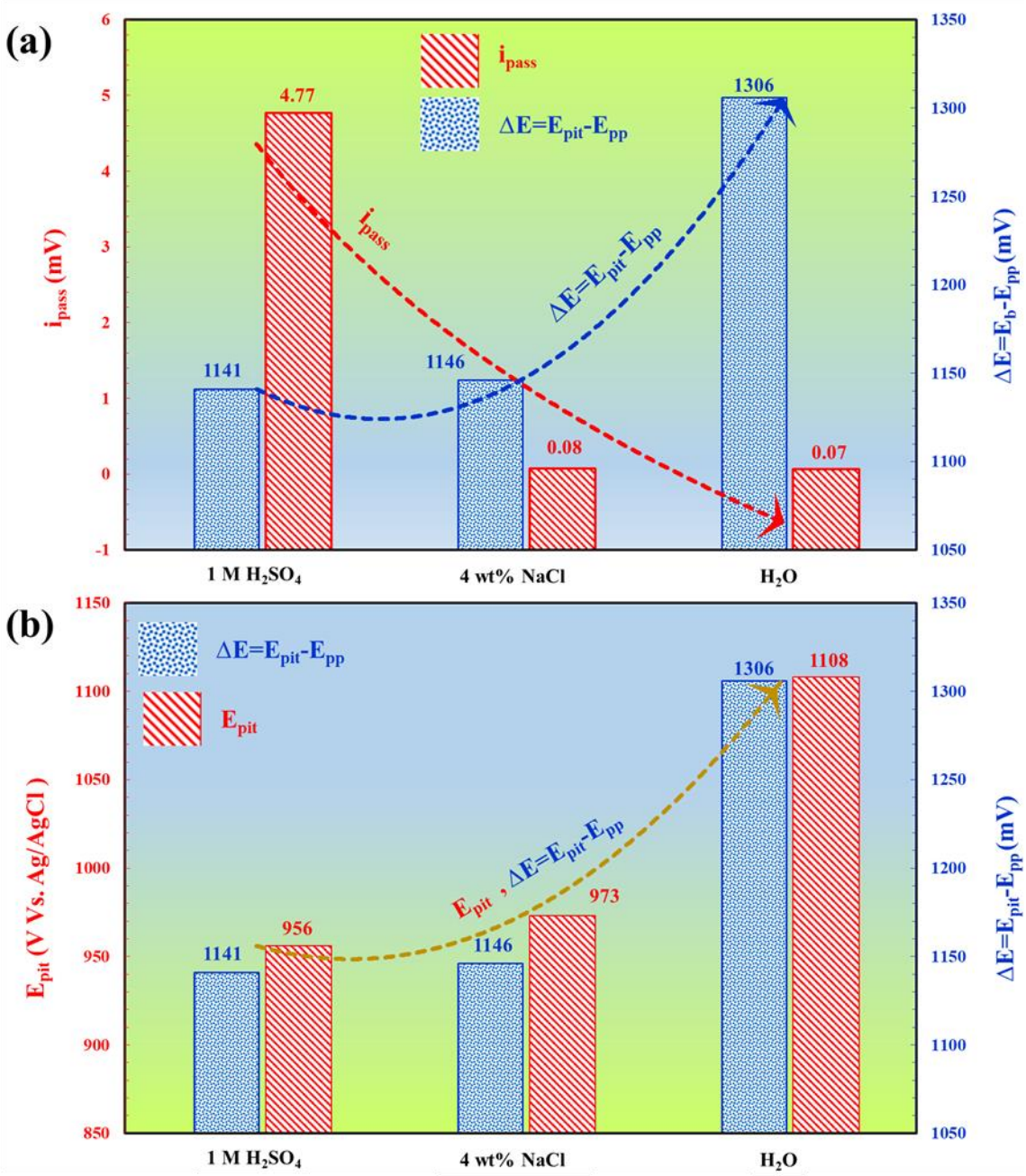


Figure 6. (a) The passive current density (i_{pass}), passivation range (ΔE_{pass}), and (b) pitting potential (E_{pit}) of the FeNiCoCr alloy in three environments: 1 M sulfuric acid, 4 wt% sodium chloride solution, and deionized water.

As shown in Figure 6a, in the 1 M H_2SO_4 environment, the curve exhibits the highest passive current density of 4.77 μA·cm^{-2}, indicating more significant metal dissolution and a narrower passivation range of 1141 mV. In contrast, the 4 wt.% NaCl solution shows notable improvement, with a significantly lower passive current density of 0.08 μA·cm^{-2} and a slightly broader passivation range of 1146 mV. The most outstanding performance is observed in the deionized water environment, which features the lowest passive current density of 0.07 μA·cm^{-2} and the widest passivation range of 1306 mV. Figure 6b further reveals a clear correlation between pitting potential and passivation range: a higher pitting potential corresponds to a broader passivation range.

These results suggests the FeCoNiCr alloy demonstrates an extraordinary capacity for passive

film formation and corrosion resistance that dynamically adapts to different environmental conditions. The progressive enhancement of passive film stability from acidic to chloride to pure water environments indicates a sophisticated corrosion protection mechanism. The decreasing passive current density and increasing passivation range reflect the alloy's ability to develop more protective and resilient passive films, with the water environment revealing the most stable and least invasive corrosion behavior, possibly due to a lower defect density or a more compact structure [4].

4. Conclusions

In this study, the microstructure and corrosion behavior of a FeCoNiCr medium-entropy alloy produced via vacuum arc melting were investigated. The key findings of this research can be summarized as follows:

1. The as-cast alloy predominantly exhibits a FCC structure, as confirmed by X-ray diffraction analysis.
2. The alloy exhibits a hierarchical microstructure, consisting of large equiaxed grains approximately 100–400 μm in size, each containing a refined cellular substructure
3. The corrosion rate of the alloy is markedly higher-by about two orders of magnitude-in 1 M sulfuric acid compared to both deionized water and a 4 wt.% sodium chloride solution. This substantial increase highlights the alloy's susceptibility to aggressive acidic environments, whereas it remains more stable in neutral or chloride-containing solutions.
4. In the sodium chloride solution, the alloy demonstrates strong corrosion resistance, characterized by a broad passivation range of 1146 mV and a low passive current density of 0.08 $\mu A \cdot cm^{-2}$. These properties indicate the formation of a stable, protective passive film, suggesting the alloy is well-suited for applications in chloride-rich environments where such passivation is critical for long-term durability.

Acknowledgements

The authors gratefully acknowledge Dr. Javid Naseri for his kind assistance in the production of the alloy.

Financial support by Shahid Chamran University of Ahvaz (Ahvaz, Iran) through grant number SCU.EM1403.222 is gratefully appreciated.

CRediT authorship contribution statement

N. Hedayati and Y. Heidari: Formal analysis, Investigation, Software. **Kh. Gheisari:** Writing – original draft, Supervision. **M. Yeganeh:** Supervision, Formal analysis.

Availability of data and material

The data would be made available by the corresponding authors on request.

Declaration of competing interest

The authors declare that they have no known competing financial interests or personal relationships that could have appeared to influence the work reported in this paper.

References

[1] M.C. Gao, J.-W. Yeh, P.K. Liaw, Y. Zhang, High-entropy alloys: fundamentals and applications, Springer, 2016.

[2] B.S. Murty, J.-W. Yeh, S. Ranganathan, P.P. Bhattacharjee, H. alloys, Elsevier, (2019).

[3] A. Mueller-Grunz, P. Alveen, S. Rassbach, R. Useldinger, S. Moseley, The manufacture and characterization of WC-(Al) CoCrCuFeNi cemented carbides with nominally high entropy alloy binders, International Journal of Refractory Metals and Hard Materials 84 (2019) 105032.

[4] Y. Heidari, K. Gheisari, M. Yeganeh, Effect of Cr content on the structure and corrosion properties of (FeCoNi) 0.75 Cu0. 25-xCrx high entropy alloys in 1 M H2SO4, Journal of Materials Research and Technology 35 (2025) 5322–5335.

[5] M. Javdan, K. Gheisari, M. Reihanian, FeCoNi) 75Cu25-xSix high entropy alloys prepared by mechanical alloying and spark plasma sintering: Microstructure, deformation behavior and dynamic recrystallization kinetics, Materials Characterization 211 (2024) 113861.

[6] F. Alijani, M. Reihanian, K. Gheisari, M. Yuasa, H. Miyamoto, Microstructural characterization of mechanically alloyed FeCoNiMnV high entropy alloy consolidated by spark plasma sintering, Advanced Engineering Materials 22 (2020) 1901311.

[7] F. Alijani, M. Reihanian, K. Gheisari, Study on phase formation in magnetic FeCoNiMnV high entropy alloy produced by mechanical alloying, Journal of Alloys and Compounds 773 (2019) 623–630.

[8] Y. Fu, J. Li, H. Luo, C. Du, X. Li, Recent advances on environmental corrosion behavior and mechanism of high-

entropy alloys, Journal of Materials Science & Technology 80 (2021) 217–233.

[9] C. Lee, C. Chang, Y. Chen, J. Yeh, H. Shih, Effect of the aluminium content of AlxCrFe1. 5MnNi0. 5 high-entropy alloys on the corrosion behaviour in aqueous environments, Corrosion Science 50 (2008) 2053–2060.

[10] X. Qiu, Y. Zhang, C. Liu, Effect of Ti content on structure and properties of Al2CrFeNiCoCuTix high-entropy alloy coatings, Journal of Alloys and Compounds 585 (2014) 282–286.

[11] S. Öztürk, F. Alptekin, S. Önal, S.E. Sünbül, Ö. Şahin, K. İçin, Effect of titanium addition on the corrosion behavior of CoCuFeNiMn high entropy alloy, Journal of Alloys and Compounds 903 (2022) 163867.

[12] D. Kumar, O. Maulik, V. Sharma, Y. Prasad, V. Kumar, Understanding the effect of tungsten on corrosion behavior of AlCuCrFeMnW x high-entropy alloys in 3.5 wt.%, NaCl Solution, Journal of Materials Engineering and Performance 27 (2018) 4481–4488.

[13] Y. Chou, J. Yeh, H. Shih, The effect of molybdenum on the corrosion behaviour of the high-entropy alloys Co1, 5CrFeNi1 5Ti0 (2010) 5.

[14] S. Yang, W. Yu, T. Liu, C. Li, Y. Zhang, Y. Qu, Effect of Cr content on corrosion behavior of AlCrxFeNi2Cu1. 6 high entropy alloys, Materials Research Express 6 (2019) 076501.

[15] H. Wang, T. Wang, Effect of boron on mechanical and anti-corrosion properties of Al0. 3CoFeMnNi high-entropy alloys, Materials Science and Technology 37 (2021) 738–744.

[16] S. Tanhaei, K. Gheisari, S.A. Zaree, Effect of cold rolling on the microstructural, magnetic, mechanical, and corrosion properties of AISI 316L austenitic stainless steel, International Journal of Minerals, Metallurgy, and Materials 25 (2018) 630–640.

[17] N. Jahani, M. Reihanian, K. Gheisari, Alloying and corrosion characteristics of FeNiMnCu-based high entropy alloys, Materials Chemistry and Physics 315 (2024) 128990.